HHS Public Access

Author manuscript

Eur J Nucl Med Mol Imaging. Author manuscript; available in PMC 2019 January 12.

Published in final edited form as:

Eur J Nucl Med Mol Imaging. 2013 July ; 40(Suppl 1): S48–S59. doi:10.1007/s00259-013-2419-6.

Functional and molecular imaging of localized and recurrent prostate cancer

Kinzya Grant,
Molecular Imaging Program, National Cancer Institute, NIH, Bethesda, MD, USA

Maria L. Lindenberg,
Molecular Imaging Program, National Cancer Institute, NIH, Bethesda, MD, USA

Haytham Shebel,
Department of Radiology, Urology and Nephrology Center, Mansoura University, Mansoura, Egypt

Yuxi Pang,
Philips Healthcare, Cleveland, OH, USA

Harsh K. Agarwal,
Philips Research North America, Briarcliff Manor, NY, USA

Marcelino Bernardo,
Molecular Imaging Program, National Cancer Institute, NIH, Bethesda, MD, USA

SAIC Frederick, NCI-Frederick, Frederick, MA 21702, USA

Karen A. Kurdziel,
Molecular Imaging Program, National Cancer Institute, NIH, Bethesda, MD, USA

Baris Turkbey, and
Molecular Imaging Program, National Cancer Institute, NIH, 10 Center Dr, MSC 1182 Bldg 10, Room B3B69, Bethesda, MD 20892-1088, USA

Peter L. Choyke
Molecular Imaging Program, National Cancer Institute, NIH, Bethesda, MD, USA

Abstract

Prostate cancer is the most common malignancy among American men. Imaging of localized and recurrent prostate cancer is challenging since conventional imaging techniques are limited. New imaging techniques such as multiparametric MRI and PET with targeted tracers have been investigated extensively in the last decade. As a result, the role of novel imaging techniques for the detection of localized and recurrent prostate cancer has recently expanded. In this review, novel functional and molecular imaging techniques used in the management of localized and recurrent prostate cancer are discussed.

Correspondence to: Baris Turkbey.

Conflicts of interest None.

Keywords

Prostate cancer; MRI; PET/CT

Introduction

Prostate cancer is currently the most commonly diagnosed solid organ malignancy in men in the developed world with a life-time risk of approximately 1 in every 6 individuals [1, 2]. Early detection of prostate cancer is important since treatment when the cancer is confined to the prostate gland can be curative, whereas treatment of later stage disease can result in increased morbidity, diminished quality of life and death. Application of PSA screening has increased the incidence of prostate cancer diagnosis, specifically early stage disease; however, the role of PSA screening in the recently observed decline in prostate cancer-specific death rates is controversial. To date, conventional imaging techniques (e.g. CT) have played a relatively minor role in the management of organ-confined prostate cancer or locally recurrent disease [3]. On the other hand, there is growing interest in the use of novel imaging techniques including multiparametric MRI (MP MRI) with anatomical and functional pulse sequences and PET/CT with novel tracers which may play a role in detection of localized and locally recurrent disease [4, 5]. In this review, novel functional and molecular imaging techniques used in the management of localized and recurrent prostate cancer are discussed.

Multiparametric MRI

MP MRI has emerged as an important method for localizing prostate cancers confined to the gland. Prostate MRI was first developed to stage prostate cancer with regard to capsular and seminal vesicle involvement. However, its role has now evolved to cancer detection. The combined use of T2-weighted (T2-W) imaging, diffusion-weighted (DW) imaging, dynamic contrast-enhanced (DCE) MRI and MR spectroscopic imaging (MRSI) has proven useful for verifying the presence of cancer, thereby guiding biopsy and subsequent therapy. Each of the four components of MP MRI are discussed in the following sections.

T2-weighted MRI

T2-W MRI is the basic imaging modality in MP MRI of the prostate. Its main role is the evaluation of the zonal anatomy of the prostate thereby permitting prostate cancer detection. T2-W MRI can clearly differentiate between the peripheral zone (PZ) and the central glands (CG) of the prostate and its capsule, and provides the highest spatial resolution for visualization of tumors and their relationship to the prostatic capsule, neurovascular bundles, anterior fibrous stroma, bladder and seminal vesicles.

Within the normally high-signal PZ the presence of a focal low signal intensity is typical of prostate cancer on T2-W MRI [6] (Fig. 1). For instance, Tamada et al. examined 50 patients with prostate cancer by T2-W MRI and found that most cancers displayed a well-circumscribed or triangular shaped area of homogeneous low signal intensity when located in the PZ [7]. In 70 patients undergoing endorectal coil MP MRI with MRI at 3 T, Turkbey

et al. found a sensitivity and specificity of T2-W MRI of 42 % and 83 %, respectively, using a stringent approach to pathological correlation. Using a less stringent approach that allowed negotiation between imaging and pathological correlation, the sensitivity and specificity of T2-W MRI were 73 % and 89 %, respectively [8]. Sensitivities do not approach 100 % because many of the cancers detected on pathological examination are microscopic and therefore undetectable by MRI. Furthermore, some tumors are “sparse”, meaning that there are islands of tumor separated by extensive normal tissue; these can be difficult to detect as well. Specificities do not approach 100 % because T2-W MRI is not specific for cancer since a similar low signal pattern is seen in various conditions such as prostatitis, benign hyperplasia, hemorrhage, atrophy, biopsy-related scars, intraepithelial neoplasia and posttreatment (hormone, ablation, etc.) changes [4]. A recent prospective study by Vargas et al. found that the diagnostic performance of T2-W MRI in detecting low risk lesions in 183 patients (low tumor volume and low Gleason score) was significantly affected if the tumor volume was less than 1 cm^3 or the Gleason score was 6 or lower [9].

Prostate cancer within the CG is more difficult to detect than PZ cancer. A major task is to differentiate benign prostatic hyperplasia (BPH), which is very common in the CG, from cancer. In their retrospective study of 148 patients with CG tumors, Akin et al. found features that favor cancer over BPH including a homogeneous low signal intensity lesion without a distinct capsule, ill-defined margins and lenticular shaped area confluent with the anterior fibromuscular stroma [10]. Moreover, Vargas et al. evaluated CG cancers in 211 patients and found that tumors that invade the CG from the PZ are more aggressive than tumors confined to the CG [11]. There is a growing consensus that T2-W MRI is the most important sequence for detecting CG tumors as the normal “checkerboard” pattern of BPH is replaced with an “erased charcoal” appearance in cancer. For instance, a recent study involving 28 patients by Hoeks et al. showed that the T2-W MRI sequence was sufficient for cancer detection in the CG and other components of the MP MRI were not as useful [12].

Complete diagnostic work-up of prostate cancer depends not only on cancer detection of suspicious areas but also on evaluation of its extension and relationship to the prostatic capsule, seminal vesicles and posterior bladder wall. Identification of any of these features can radically alter the treatment strategy and prognosis [13].

The typical finding of extracapsular extension (ECE) is the direct extension of the tumor into periprostatic fat. However, direct extension cannot be seen in all situations and secondary findings of ECE are asymmetry of the neurovascular bundle, contour angulation and bulging, an irregular capsule, capsular retraction or obliteration of the rectoprostatic angle [6, 14]. In a cohort of 32 patients, Bloch et al. found mean sensitivity, specificity, and positive and negative predictive values for assessment of ECE of 86 %, 95 %, 90 %, and 93 %, respectively [14]. Criteria for seminal vesicle invasion include direct extension of the tumor into one or both seminal vesicles and/or the presence of focal low signal intensity filling defects within the normally hyperintense seminal vesicles [6, 15]. In a series of 354 men, Sala et al. found sensitivity and specificity of MRI for the detection of seminal vesicle invasion of 79 % and 99 %, respectively [15]. Finally, direct extension of prostate cancer into the bladder base portends a difficult clinical course and may require more radical surgical or radiation methods.

Tumor recurrence may occur in the prostatic bed once the prostate has been surgically removed or has been irradiated. MP MRI is considered an alternative viable tool for the detection of tumor recurrence when there is biochemical evidence (rising PSA levels) of residual or recurrent localized disease after radical prostatectomy, external beam radiation, androgen-deprivation therapy and/or focal therapy (Fig. 2). After radical prostatectomy, tumor recurrence appears on T2-W MRI as a hyperintense soft-tissue mass in the prostatic fossa in comparison to the pelvic muscle signal intensity. However, postoperative fibrosis can mimic tumor and T2 alone is insufficient to diagnose local recurrence [16]. Cirillo et al. evaluated T2-W MRI in 72 patients with biochemical recurrence (BCR) and found a sensitivity and specificity of 61.4 % and 82.1 %, respectively [17]. Similarly, Casciani et al. evaluated T2-W MRI in 46 patients with BCR and found a sensitivity and specificity of only 48 % and 52 %, respectively [18]. Thus, while recurrences can be detected with T2-W MRI alone, it is not ideal.

Recurrences can also be detected after radiation therapy (RT). RT usually reduces the tumor size and signal intensity on T2-W MRI. When local recurrence is suspected after RT, the suspicious area is recognized as a nodular lesion of lower signal intensity than normal prostatic tissue which increases in size over time and may exhibit a capsular bulge. Although it may seem obvious, a baseline study demonstrating the site of the primary tumor can be very helpful in identifying recurrence, as the most common site of recurrence is the primary site. T2-W MRI as a single modality has marked limitations for detecting postradiation recurrences. Westphalen et al. examined 64 patients with suspicion of recurrence after RT and found that the area under the receiver operating characteristic (ROC) curve (AUC) was only 0.67 when using T2-W MRI alone for cancer recurrence detection [19]. Thus, in many patients detection of recurrent tumor by T2-W MRI is difficult and DCE MRI has proven more reliable in this setting. This is discussed in more detail in subsequent sections.

Focal therapy is emerging as an alternative treatment for localized prostate cancer in low-risk disease. A number of different focal therapies currently exist including cryotherapy, high-intensity focused ultrasound (HIFU), focal laser ablation and photodynamic therapy. Tumor recurrence in patients following focal therapy can be difficult to assess as the therapy itself induces alterations in the architecture of the tissue that could mimic tumor. Most focal therapies result in low signal intensity changes on T2-W MRI making differentiation between treatment effects and tumor recurrence difficult [15]. Since focal therapy is a relatively new approach to prostate cancer management, more experience is needed to evaluate the utility of MP MRI in monitoring follow-up and evaluating for residual/recurrent disease.

Diffusion-weighted MRI

DW MRI depicts the motion of water protons in tissue by applying a series of lower and higher magnetic field gradients, denoted as “b” values. This technique was initially introduced for the imaging of acute stroke. However, recently, it has found utility in cancer imaging [20]. In prostate cancer imaging, DW MRI has become a noninvasive adjunct to T2-W MRI and has quickly gained a major role in MP MRI to aid in the detection and characterization of prostate cancer. Malignant cell growth is associated with higher cell

density which restricts water molecule movement, hence reducing water diffusion. This can be represented on a map of apparent diffusion coefficients (ADC) which are calculated from multiple b-value DW MR images [21]. Since the PZ of the prostate normally demonstrates relatively high water diffusion, tumors are relatively easily seen as low signal against a background of high signal in the PZ [22] (Figs. 1 and 3). The CG of the prostate is more heterogeneous as ADC values of BPH vary with the type of hyperplastic change (stromal vs. glandular), and this makes the evaluation of DW MRI findings of the CG more challenging [23, 24]. CG tumors also appear hypointense on ADC maps, but the anatomical context of these lesions needs to be evaluated by T2-W MRI. For instance, if the region of low signal intensity on the ADC map corresponds to a well-circumscribed BPH nodule it can be safely considered benign. Thus, DW imaging must be interpreted in combination with T2-W MRI to increase the accuracy of prostate cancer detection. In doing so, mimics of prostate cancer on ADC maps such as hemorrhage, prostatitis, BPH nodules, dysplasia and high-grade prostatic intraepithelial neoplasia, and posttreatment changes may be revealed.

In a study of 49 patients who underwent radical prostatectomy following MRI, Oto et al. analyzed the diffusion parameters of CG prostate cancer, stromal hyperplasia (SH), and glandular hyperplasia (GH) in the differentiation of CG cancer from benign CG hyperplasia. On the basis of histopathological correlation, 38 foci of carcinoma, 38 SH nodules, and 38 GH nodules in the CG were localized. ROC and multivariate logistic regression analyses were performed for differentiation of CG cancer from the SH and GH foci. The average ADCs were 1.05, 1.27 and 1.73, in CG carcinoma, SH foci and GH foci, and differed significantly, yielding ROC curve AUCs of 0.99 and 0.78, respectively, for differentiation of carcinoma from GH and SH [23]. However, in individual patients the ADCs can overlap between cancer and hyperplastic nodules leading to uncertainty based on ADC values alone. This is why ADC maps must be viewed in the context of the anatomy.

DW imaging is known to provide better detection of prostate cancer than T2-W imaging alone in both localized and recurrent prostate cancer. Wu et al. conducted a 10-year meta-analysis evaluating the diagnostic performance of T2-W imaging in combination with DW imaging in detecting prostate carcinoma. The pooled sensitivity and specificity of DW added to T2-W imaging was 76 % (65–84 %) and 82 % (77–87 %), respectively [25]. Others have found an advantage in adding DW MRI to the MP MRI. Haider et al. performed a prospective trial in 49 patients prior to radical prostatectomy using an endorectal coil at 1.5 T. T2-W MRI alone and then T2-W MRI images plus ADC maps (T2 + DW imaging) were scored for the likelihood of tumor and were compared with whole-mount histology. On a “per prostate” basis, the sensitivity was significantly higher with T2-W + DW imaging (81 %) vs. T2-W imaging alone (54 %), with T2-W plus DW imaging showing slightly lower specificity than T2-W imaging alone (84 % versus 91 %, respectively) [26].

Many investigators have noted the relationship between ADC values and Gleason score of prostate cancer. The ability to predict tumor aggressiveness could be useful in selecting appropriate therapies [27, 28]. In a study by Hambrock et al., 51 patients with prostate cancer underwent MR imaging, including DW MRI, before prostatectomy. Tumors identified in prostatectomy specimens were classified qualitatively as low, intermediate or high grade based on Gleason score. The median ADC in the tumors showed a negative

relationship with Gleason score, and the differences were statistically significant. The authors concluded that ADC values show an inverse relationship to Gleason score in PZ prostate cancer [27]. Several other authors have shown that this relationship holds true in the PZ of the prostate with MRI at both 1.5 T and 3 T. However, while the differences between the groups were statistically significant, there remained some overlap between Gleason score and ADC values, thus limiting its predictive value in an individual patient.

The role of DW imaging is of particular interest in the setting of BCR after RT. In a prospective study of 36 consecutive patients with BCR after RT, Kim et al. correlated MRI findings with transrectal biopsy in 18 patients, and found 65 of 216 prostate sectors (30 %) positive for cancer. They found that T2-W and DW imaging combined showed a greater sensitivity than T2-WI alone for the prediction of recurrent cancer as well as a significantly greater ROC curve AUC [29]. DW imaging in conjunction with T2-W MRI and DCE MRI was also shown to aid in the identification of locally recurrent disease after treatment with HIFU in 27 patients with a reported sensitivity range of 63–87 % [30].

Recent studies emphasize the effects of varying the diffusion sensitizing gradient (b-values) to optimize detection and characterization of prostate lesions [31, 32]. For example, “high” b-values of 1,000 and 2,000 have been suggested to improve the utility of DW-MRI. These higher b-values can only be obtained at the cost of noisier images with lower signal to noise ratios. Further research is needed in this area to confirm early results including the use “calculated high b-value” imaging derived from actual imaging with lower b-values. Additionally, it is possible to extract from DW-MRI a small perfusion component that may be diagnostically meaningful. Thus, there is interest in exploring low b-values where the effects of perfusion are most detectable. Le Bihan et al. proposed a method for measuring a pseudodiffusion effect caused by blood perfusion. The proposed method is called “intravoxel incoherent motion” (IVIM), and has been applied to prostate imaging [33]. Pang et al. demonstrated that the inclusion of high b-value diffusion data in IVIM modeling can compromise the IVIM-derived perfusion parameter for distinguishing between normal tissue and tumor. To facilitate IVIM analysis of multi-b-value data, including higher b-values (>700 s/mm^2), an additional contribution from so-called non-Gaussian diffusion was proposed. Non-Gaussian diffusion is believed to be caused by the presence of different barriers in complex structures, which prevent water molecules from moving freely along predicted Brownian motion paths [34]. IVIM measurements can be incorporated into the current MP paradigm for diagnosing prostate cancer with MRI and could, in theory, reduce or eliminate the need for gadolinium-enhanced DCE MRI, which is especially relevant in patients who cannot receive intravenous a gadolinium-based contrast agent (GBCA) [34]. However, IVIM-related changes are relatively small and thus difficult to detect.

The literature shows a renewed interest in defining monoexponential versus biexponential behavior, as small b-values are known to depict changes in microcirculation [34]. In addition, computed b-values in oncological imaging have been described as a means to improve lesion detection [35].

Magnetic resonance spectroscopic imaging

Proton MRSI is a method of MR acquisition that displays the relative concentrations of chemical metabolites such as citrate, creatine, choline and polyamines. Normal prostate contains high concentrations of citrate and polyamines, whereas choline and creatine levels are relatively low. Prostate tumors are marked by increased levels of choline, secondary to cell turnover and neoplastic proliferation. Decreased citrate levels are associated with abnormally functioning cancer cells. Thus, increases in the ratio of choline to citrate ((choline+creatine)/citrate or choline/citrate) are a marker of prostate cancer [36] (Fig. 3).

Early studies utilizing MRSI were performed at 1.5 T, but since MRSI is improved significantly at higher field strengths, much of the later work has been performed at 3 T [37–39]. MRSI has been shown to aid in tumor localization and characterization [40, 41]. When positive, MRSI is predictive of higher tumor grade and/or increased tumor volume. This assessment can lead to changes in clinical management [42]. In the diagnosis of ECE, the addition of MRSI reportedly improves the accuracy of less experienced readers [43]. Several authors have confirmed the potential of MRSI in the assessment of prostate cancer aggressiveness. However, considerable overlap among different grades of tumor remains, and interpretation of MR spectra is difficult [44, 45]. MRSI has also been incorporated into predictive nomograms that are used to advise patients about the likelihood that advanced disease exists. Among 181 patients with low-risk prostate cancer, Shukla-Dave et al. sought to validate previously published nomograms that incorporated clinical data (age, PSA, symptoms etc), percentage of biopsy cores positive and MRI or MRI/MRSI results to predict insignificant prostate cancer. The authors also designed new nomograms incorporating MR results and clinical data without detailed biopsy data. The models based on MR or MRSI performed significantly better than those based on simple clinical data alone ($P \leq 0.05$) although performance was comparable when more complex clinical data were incorporated into the nomogram [46]. Nonetheless, technical challenges associated with obtaining clean MR spectra, often requiring the assistance of an on-site MR physicist, has limited the adoption of this method.

The role of MRSI in BCR deserves special attention. Westphalen et al. investigated MRSI in the evaluation of recurrence in 26 patients after external beam RT. Transrectal ultrasound-guided biopsy was the reference standard. The ROC curve AUC of MRSI was a respectable 83.0 %. There was no significant improvement with the combination of all MR techniques beyond the accuracy of MRSI alone; however, a trend toward improved discrimination was noted (86.9 %; $P=0.09$) [19, 47]. MRSI has also been investigated in the setting of BCR after radical prostatectomy and during androgen-deprivation therapy [48, 49], but results were not conclusive and technical factors weigh against its use [50].

Dynamic contrast-enhanced MRI

DCE MRI is the rapid acquisition of short T1-W images before, during and after the bolus administration of a GBCA. The main value of DCE MRI is its ability to detect abnormal tumor vascularity and permeability. The normal prostate is a relatively vascular organ and therefore, in order to detect subtle increases in vascularity, imaging must be conducted

quickly after a rapid bolus of GBCA [51]. It is relatively easy to perform and can be successfully integrated at most medical centers.

DCE MRI is typically acquired with fast serial three-dimensional acquisitions and an injection rate of 2–4 ml/s followed by a 20-ml saline flush. Usually, early enhancement is detected when images are acquired every 5 s or less over a period of approximately 5 min. The GBCA rapidly leaks into the extravascular extracellular space of the tumor and is reflected in a rapid enhancement of the lesion. The signal measured on DCE MRI is always a combination of perfusion and permeability (leakiness) of the cancer vascularity [51] (Figs. 1 and 3).

There are three generally accepted approaches to the analysis and interpretation of DCE MRI: qualitative, semiquantitative and quantitative. Qualitative analysis is the visual detection of focal early and intense enhancement with early washout compared to normal prostatic tissue [13]. Semiquantitative analysis is based on assessment of the time signal curve and includes such measurements as the AUC, time to peak enhancement, and initial slope. Enhancement curves can be classified into three types of dynamic curve: persistent increase (type 1), plateau (type 2), and decline after initial upslope (type 3). Of these curves, type 3 is most commonly associated with prostate cancer, although mixtures of different curves are often found within lesions. This approach is considered semiquantitative (and therefore more difficult to reproduce) because it depends on the rate of injection, cardiovascular status of the patient and the temporal resolution of the image acquisition [52, 53]. The large number of parameters and acquisition methods used for DCE MRI has made standards difficult to agree upon.

Quantitative methods depend on analysis of concentration changes of gadolinium within the lesion and utilize one of several multicompartment pharmacokinetic models [51]. Most of these models assume that GBCAs leak from the blood pool to the extravascular extracellular space and then leak back into the blood pool, while also steadily being excreted via the kidneys. The most widely used model is the Toft's model which describes the transfer of GBCA from the vascular compartment to the tumor compartment (k-trans representing forward vascular permeability and flow), reverse transfer of contrast from the extracellular space back to the plasma space (k_{ep} representing backward leakage) and the fraction of plasma volume compared to whole tissue volume (fpV) and the fraction of tumor volume occupied by extravascular extracellular space (V_e) [54]. In prostate cancer, k-trans and k_{ep} tend to be higher than in normal tissue; however, there may be overlap between benign and malignant tissues, especially in the CG [54].

Several studies have shown a high sensitivity of DCE MRI in comparison to T2-W MRI for prostate cancer localization. For instance, in 50 patients undergoing surgery, Ocak et al. found the sensitivity and specificity of DCE MRI to be 73 % and 88 %, respectively [55]. Delongchamps et al. evaluated MP MRI at 3 T in 57 patients prior to surgery and found that the combination of DCE MRI and T2-W MRI significantly improved cancer detection sensitivity from 63 % to 79–81 % in the PZ [56]. The limitations of DCE MRI are its inability to discriminate cancer from other highly vascular abnormalities such as prostatitis especially in the PZ and from BPH nodules in the CG.

DCE MRI is the most important MR sequence in the setting of BCR following radical prostatectomy. Delayed postoperative changes show either no enhancement or mild enhancement on DCE MRI while recurrent tumors show intense, focal enhancement in early phases and rapid washout in the venous phase [57]. In 46 patients with BCR after radical prostatectomy, Casciani et al. found that DCE MRI, alone or in combination with T2-W MRI, improved sensitivity from 48–52 % to 88–100 % [18]. In suspected tumor recurrence after RT, DCE MRI has been reported to improve the sensitivity and specificity (Fig. 2). In 33 patients with BCR after RT, Haider et al. found that DCE MRI improved the results compared with T2-W MRI alone with significantly better sensitivity (72 % versus 38 %), positive predictive value (46 % versus 24 %) and negative predictive value (95 % versus 88 %) [52]. DCE MRI may also be useful in assessing the prostate following focal therapy. For instance, after HIFU in 27 patients, Kim et al. evaluated DCE MRI and T2-W MRI for the detection of recurrent tumors in treated patients and found that DCE MRI was more sensitive than T2-W MRI with DW imaging, although T2-W MRI with DW imaging was still more specific for recurrence than DCE MRI [30].

Comparison of MRI and PET/CT

In theory, PET/CT provides the best of both worlds: the very high sensitivity of PET and the high resolution of CT. Indeed, PET/CT has provided a noninvasive method to diagnose and stage malignancies, primarily with the radiotracer ^{18}F-FDG, leading to its incorporation into standard work-ups of many cancer types. Unfortunately, this agent has not been uniformly successful with all cancers, one of which is prostate cancer. Nevertheless as demonstrated in Fig. 4, ^{18}F-FDG may be useful in selected patients with aggressive primary disease and later stages of the disease [58, 59].

The relative failure of ^{18}F-FDG in prostate cancer has led to the development of other radiotracers. One of the challenges with organ-confined prostate cancer is distinguishing benign conditions such as prostatitis and BPH from tumor. The radiopharmaceutical ^{11}C-choline has been extensively studied in prostate cancer. As a precursor of cell membrane phospholipids, choline is taken up by prostate cancers. Hara et al. were among the first to demonstrate that ^{11}C-choline can show prostate cancer confined to the gland and local metastasis [60]. Its role in primary prostate cancer is controversial as it displays a high rate of false-negative results when analyzed in comparison with histopathology for prostate cancer and up-take in benign prostatic conditions [61]. Eschmann et al. compared ^{11}C-choline and whole-body MRI in a mixed group of patients who were newly diagnosed or had definitive therapy but rising PSA levels. In this study, sensitivity and accuracy were higher with ^{11}C-choline (96.6 % and 93.3 %) than with whole-body MRI (78.4 % and 81 %). However, specificity was better with whole-body MRI (94.1 %) than with ^{11}C-choline (76.5 %), suggesting that their combined use may be beneficial [62]. Others have also suggested that ^{11}C-choline may be superior to MRI in some settings. Yamaguchi et al. evaluated ^{11}C-choline PET in comparison with MRI and proton MRSI and found PET to have a diagnostic sensitivity of 100 % in large primary lesions, while MRI and MRSI had sensitivities of only 60 % and 65 % respectively, and in general, the performance of MRI was better than, or equal to, that of ^{11}C-choline PET/CT [63]. Beer et al. examined ^{11}C-choline in relation to DW MRI in a mixed group of 14 patients with prostate cancer and

found a moderate inverse correlation between the two. Lymph nodes with low ADC values had higher standardized uptake values, suggesting malignant disease [64]. Recently, Park et al. coregistered MP MRI with ^{11}C-choline PET to obtain parametric fusion PET/MRI images based on ^{11}C-choline PET/CT and ADC maps. The combination of these modalities resulted in improved target to background contrast for tumors with a Gleason score of 3+4 or above compared to either modality alone [65].

^{11}C-acetate PET/CT is another radiotracer that has been studied in prostate cancer. Acetate is a naturally occurring fatty acid precursor that is converted to acetyl-CoA, a substrate for the tricarboxylic acid cycle, by fatty acid synthase. Acetyl-CoA is incorporated into cholesterol and fatty acids, and therefore ^{11}C-acetate uptake is an indirect biomarker of fatty acid synthesis. ^{11}C-acetate shares many characteristics with ^{11}C-choline, notably the inability to differentiate tumor from benign tissue within the gland [66]. Mena et al. evaluated the use of ^{11}C-acetate PET/CT in patients with localized disease and demonstrated higher uptake in intraprostatic tumor foci than in normal prostate tissue; however, uptake in tumors was similar to that in BPH nodules. Analysis demonstrated that ^{11}C-acetate PET/CT was inferior to MP MRI for prostate lesions greater than 0.5 cm; however, when only lesions greater than 0.9 cm were considered, detection rates were comparable for the two modalities. There was no correlation between ^{11}C-acetate uptake, PSA, or Gleason scores [67]. In patients with untreated prostate cancer, Jambor et al. found that fused data from contrast-enhanced MRI and ^{11}C-acetate PET showed better sensitivity (90 %), specificity (72 %) and accuracy (85 %) than each modality alone [68]. The same group also evaluated the ability of ^{11}C-acetate PET/CT, MRI and proton MRSI ((1)H-MRS) to image localized prostate cancer and detect its aggressiveness, using qualitative and quantitative approaches in 21 patients. The sensitivity, specificity and accuracy of ^{11}C-acetate PET/CT at the lobar level using visual analysis were 80 %, 29 %, 71 %, respectively, and of contrast-enhanced MRI were 89 %, 29 %, 79 %, respectively. On the other hand, the sensitivity and accuracy of ^{11}C-acetate PET/CT decreased to 64 % and 63 % and the specificity increased to 62 % when sextant analysis was performed. They concluded that ^{11}C-acetate PET/CT, MRI and (1)H-MRS can enable detection of localized prostate cancer with comparable and limited accuracy, but they fail to provide information on cancer aggressiveness [69]. Wachter et al. evaluated prostate cancer patients with elevated PSA levels after primary therapy by retrospectively fusing ^{11}C-acetate PET data with either CT or MRI data if suspicious uptake was seen on PET [70]. The combined use of functional and anatomic imaging improved diagnostic interpretation and influenced clinical management.

Another promising PET imaging agent, originally developed at Emory University, is anti-^{18}F-FACBC, which is a synthetic leucine analog that is taken up by cells via amino acid transporters. Schuster et al. showed its usefulness in assessing primary prostate cancer and metastatic/recurrent prostate cancer in the prostate bed, lymph nodes and bone [71, 72]. In localized prostate cancer, anti-^{18}F-FACBC up-take in tumor has been found to be similar to that in BPH, with a sensitivity and specificity comparable to that of MRI in tumors >0.5 cm. We and others are currently exploring the ability of anti-^{18}F-FACBC to identify lesions in patients with occult residual/recurrent prostate cancer.

As prostate cancer often metastasizes to bone, bone-seeking radiotracers are of relevance in metastatic prostate cancer. The utility of ^{18}F-NaF PET/CT is shown in Fig. 5. Mosavi et al. compared DW MRI and ^{18}F-NaF for detection of bone metastases in patients with high-risk prostate cancer and found that ^{18}F-NaF PET/CT had better sensitivity but lower specificity than whole-body DW MRI [73]. Repeated baseline studies with ^{18}F-NaF showed high intraclass correlations (>0.9) and relatively low critical percentage change (the value above which a change can be considered real) for these parameters. The tumor-to-normal bone ratio, based on the maximum standardized uptake values of identified malignant lesions, decreased with time; however, this difference was small, estimated at approximately 0.16 %/min in the first hour. Thus, the optimal uptake period is approximately 60±30 min and is relatively insensitive to minor changes in uptake period [74]. The nature of PET/CT data lends itself to automated analysis of total bone metastatic burden, and research in this area is being conducted. However, a central limitation of all bone-scanning agents, including PET-based agents, is that they indicate the metabolic activity of bone, rather than tumor.

Conclusion

Because prostate cancer is a leading cause of cancer death in men, it is important to develop appropriate imaging methods to identify disease that is still localized to the gland and define the extent of disease, thus enabling identification of extraprostatic spread or recurrence after treatment. The imaging of localized and recurrent prostate cancer has a number of limitations, but recent developments in imaging technologies, especially MRI, and the emergence of targeted imaging with novel PET tracers could lead to significant improvements in prostate cancer detection, and may therefore allow more accurate diagnosis. Several PET radio-tracers used in prostate cancer are effective in identifying metastatic and recurrent disease in definitively treated patients, but the quest continues for an optimal PET imaging agent specific for tumor within the gland. Hopefully, the advent of hybrid PET/MR technology will expand the advantages of both PET and MRI to improve characterization of prostate cancer.

References

1. Jemal A, Bray F, Center MM, Ferlay J, Ward E, Forman D. Global cancer statistics. CA Cancer J Clin. 2011;61:69–90. [PubMed: 21296855]
2. Siegel R, Naishadham D, Jemal A. Cancer statistics, 2012. CA Cancer J Clin. 2012;62:10–29. [PubMed: 22237781]
3. Rørvik J, Halvorsen OJ, Espeland A, Haukaas S. Inability of refined CT to assess local extent of prostatic cancer. Acta Radiol. 1993;34:39–42. [PubMed: 8427747]
4. Turkbey B, Bernardo M, Merino MJ, Wood BJ, Pinto PA, Choyke PL. MRI of localized prostate cancer: coming of age in the PSA era. Diagn Interv Radiol. 2012;18:34–45. [PubMed: 21922459]
5. Bouchelouche K, Turkbey B, Choyke P, Capala J. Imaging prostate cancer: an update on positron emission tomography and magnetic resonance imaging. Curr Urol Rep. 2010;11:180–90. [PubMed: 20425625]
6. Barentsz JO, Richenberg J, Clements R, Choyke P, Verma S, Villeirs G, et al. ESUR prostate MR guidelines 2012. Eur Radiol. 2012;22:746–57. [PubMed: 22322308]
7. Tamada T, Sone T, Higashi H, Jo Y, Yamamoto A, Kanki A, et al. Prostate cancer detection in patients with total serum prostate-specific antigen levels of 4–10 ng/mL: diagnostic efficacy of diffusion-weighted imaging, dynamic contrast-enhanced MRI, and T2-weighted imaging. AJR Am J Roentgenol. 2011;197:664–70. [PubMed: 21862809]

8. Turkbey B, Pinto PA, Mani H, Bernardo M, Pang Y, McKinney YL, et al. Prostate cancer: value of multiparametric MR imaging at 3T for detection – histopathologic correlation. Radiology. 2010;255:89–99. [PubMed: 20308447]
9. Vargas HA, Akin O, Shukla-Dave A, Zhang J, Zakian KL, Zheng J, et al. Performance characteristics of MR imaging in the evaluation of clinically low-risk prostate cancer: a prospective study. Radiology. 2012;265:478–87. [PubMed: 22952382]
10. Akin O, Sala E, Moskowitz CS, Kuroiwa K, Ishill NM, Pucar D, et al. Transition zone prostate cancers: features, detection, localization, and staging at endorectal MR imaging. Radiology. 2006;239:784–92. [PubMed: 16569788]
11. Vargas HA, Akin O, Franiel T, Goldman DA, Udo K, Touijer KA, et al. Normal central zone of the prostate and central zone involvement by prostate cancer: clinical and MR imaging implications. Radiology. 2012;262:894–902. [PubMed: 22357889]
12. Hoeks CM, Hambrock T, Yakar D, Hulsbergen-van de Kaa CA, Feuth T, Witjes JA, et al. Transition zone prostate cancer: detection and localization with 3-T multiparametric MR imaging. Radiology. 2013;266:207–17. [PubMed: 23143029]
13. Turkbey B, Choyke PL. Multiparametric MRI and prostate cancer diagnosis and risk stratification. Curr Opin Urol. 2012;22:310–5. [PubMed: 22617060]
14. Bloch BN, Furman-Haran E, Helbich TH, Lenkinski RE, Degani H, Kratzik C, et al. Prostate cancer: accurate determination of extracapsular extension with high-spatial-resolution dynamic contrast-enhanced and T2-weighted MR imaging: initial results. Radiology. 2007;245:176–85. [PubMed: 17717328]
15. Sala E, Akin O, Moskowitz CS, Eisenberg HF, Kuroiwa K, Ishill NM, et al. Endorectal MR imaging in the evaluation of seminal vesicle invasion: diagnostic accuracy and multivariate feature analysis. Radiology. 2006;238:929–37. [PubMed: 16424250]
16. Vargas HA, Wassberg C, Akin O, Hricak H. MR imaging of treated prostate. Cancer Radiol. 2012;262:26–42.
17. Cirillo S, Petracchini M, Scotti L, Gallo T, Macera A, Bona MC, et al. Endorectal magnetic resonance imaging at 1.5 Tesla to assess local recurrence following radical prostatectomy using T2-weighted and contrast-enhanced imaging. Eur Radiol. 2009;19:761–9. [PubMed: 18825386]
18. Casciani E, Polettini E, Carmenini E, Floriani I, Masselli G, Bertini L, et al. Endorectal and dynamic contrast-enhanced MRI for detection of local recurrence after radical prostatectomy. AJR Am J Roentgenol. 2008;190:1187–92. [PubMed: 18430830]
19. Westphalen AC, Coakley FV, Roach M, 3rd, McCulloch CE, Kurhanewicz J. Locally recurrent prostate cancer after external beam radiation therapy: diagnostic performance of 1.5-T endorectal MR imaging and MR spectroscopic imaging for detection. Radiology. 2010;256:485–92. [PubMed: 20551184]
20. Padhani AR, Liu G, Koh DM, Chenevert TL, Thoeny HC, Takahara T, et al. Diffusion-weighted magnetic resonance imaging as a cancer biomarker: consensus and recommendations. Neoplasia. 2009;11:102–25. [PubMed: 19186405]
21. Zelhof B, Pickles M, Liney G, Gibbs P, Rodrigues G, Kraus S, et al. Correlation of diffusion-weighted magnetic resonance data with cellularity in prostate cancer. BJU Int. 2009;103:883–8. [PubMed: 19007373]
22. Gibbs P, Tozer DJ, Liney GP, Turnbull LW. Comparison of quantitative T2 mapping and diffusion-weighted imaging in the normal and pathologic prostate. Magn Reson Med. 2001;46:1054–8. [PubMed: 11746568]
23. Oto A, Kayhan A, Jiang Y, Tretiakova M, Yang C, Antic T, et al. Prostate cancer: differentiation of central gland cancer from benign prostatic hyperplasia by using diffusion-weighted and dynamic contrast-enhanced MR imaging. Radiology. 2010;257:715–23. [PubMed: 20843992]
24. Tamada T, Sone T, Toshimitsu S, Imai S, Jo Y, Yoshida K, et al. Age-related and zonal anatomical changes of apparent diffusion coefficient values in normal human prostatic tissues. J Magn Reson Imaging. 2008;27:552–6. [PubMed: 18219616]
25. Wu LM, Xu JR, Ye YQ, Lu Q, Hu JN. The clinical value of diffusion-weighted imaging in combination with T2-weighted imaging in diagnosing prostate carcinoma: a systematic review and meta-analysis. AJR Am J Roentgenol. 2012;199:103–10. [PubMed: 22733900]

26. Haider MA, van der Kwast TH, Tanguay J, Evans AJ, Hashmi AT, Lockwood G, et al. Combined T2-weighted and diffusion-weighted MRI for localization of prostate cancer. AJR Am J Roentgenol. 2007;189:323–8. [PubMed: 17646457]
27. Hambrock T, Somford DM, Huisman HJ, van Oort IM, Witjes JA, Hulsbergen-van de Kaa CA, et al. Relationship between apparent diffusion coefficients at 3.0-T MR imaging and Gleason grade in peripheral zone prostate cancer. Radiology. 2011;259:453–61. [PubMed: 21502392]
28. Turkbey B, Shah VP, Pang Y, Bernardo M, Xu S, Kruecker J, et al. Is apparent diffusion coefficient associated with clinical risk scores for prostate cancers that are visible on 3-T MR images? Radiology. 2011;258:488–95. [PubMed: 21177390]
29. Kim CK, Park BK, Lee HM. Prediction of locally recurrent prostate cancer after radiation therapy: incremental value of 3T diffusion-weighted MRI. J Magn Reson Imaging. 2009;29:391–7. [PubMed: 19161194]
30. Kim CK, Park BK, Lee HM, Kim SS, Kim E. MRI techniques for prediction of local tumor progression after high-intensity focused ultrasonic ablation of prostate cancer. AJR Am J Roentgenol. 2008;190:1180–6. [PubMed: 18430829]
31. Metens T, Miranda D, Absil J, Matos C. What is the optimal b-value in diffusion-weighted MR imaging to depict prostate cancer at 3T? Eur Radiol. 2012;22:703–9. [PubMed: 21971824]
32. Mazaheri Y, Vargas HA, Akin O, Goldman DA, Hricak H. Reducing the influence of b-value selection on diffusion-weighted imaging of the prostate: evaluation of a revised monoexponential model within a clinical setting. J Magn Reson Imaging. 2012;35:660–8. [PubMed: 22069141]
33. Le Bihan D, Breton E, Lallemand D, Aubin ML, Vignaud J, Laval-Jeantet M. Separation of diffusion and perfusion in intravoxel incoherent motion MR imaging. Radiology. 1988;168:497–505. [PubMed: 3393671]
34. Pang Y, Turkbey B, Bernardo M, Kruecker J, Kadoury S, Merino MJ, et al. Intravoxel incoherent motion MR imaging for prostate cancer: an evaluation of perfusion fraction and diffusion coefficient derived from different b-value combinations. Magn Reson Med. 2013;69:553–62. [PubMed: 22488794]
35. Blackledge MD, Leach MO, Collins DJ, Koh DM. Computed diffusion-weighted MR imaging may improve tumor detection. Radiology. 2011;261:573–81. [PubMed: 21852566]
36. Mazaheri Y, Shukla-Dave A, Hricak H, Fine SW, Zhang J, Inurrigarro G, et al. Prostate cancer: identification with combined diffusion-weighted MR imaging and 3D 1H MR spectroscopic imaging – correlation with pathologic findings. Radiology. 2008;246:480–8. [PubMed: 18227542]
37. McLean MA, Barrett T, Gnanapragasam VJ, Priest AN, Joubert I, Lomas DJ, et al. Prostate cancer metabolite quantification relative to water in 1H-MRSI in vivo at 3 Tesla. Magn Reson Med. 2011;65:914–9. [PubMed: 21413057]
38. Yakar D, Heijmink SW, Hulsbergen-van de Kaa CA, Huisman H, Barentsz JO, Futterer JJ, et al. Initial results of 3-dimensional 1H-magnetic resonance spectroscopic imaging in the localization of prostate cancer at 3 Tesla: should we use an endorectal coil? Invest Radiol. 2011;46:301–306. [PubMed: 21217527]
39. Yerram NK, Volkin D, Turkbey B, Nix J, Hoang AN, Vourganti S, et al. Low suspicion lesions on multiparametric magnetic resonance imaging predict for the absence of high-risk prostate cancer. BJU Int. 2012;110(11 Pt B):E783–8. [PubMed: 23130821]
40. Coakley FV, Kurhanewicz J, Lu Y, Jones KD, Swanson MG, Chang SD, et al. Prostate cancer tumor volume: measurement with endorectal MR and MR spectroscopic imaging. Radiology. 2002;223:91–7. [PubMed: 11930052]
41. Futterer JJ, Heijmink SW, Scheenen TW, Veltman J, Huisman HJ, Vos P, et al. Prostate cancer localization with dynamic contrast-enhanced MR imaging and proton MR spectroscopic imaging. Radiology. 2006;241:449–58. [PubMed: 16966484]
42. Turkbey B, Mani H, Shah V, Rastinehad AR, Bernardo M, Pohida T, et al. Multiparametric 3T prostate magnetic resonance imaging to detect cancer: histopathological correlation using prostatectomy specimens processed in customized magnetic resonance imaging based molds. J Urol. 2011;186:1818–24. [PubMed: 21944089]

43. Yu KK, Scheidler J, Hricak H, Vigneron DB, Zaloudek CJ, Males RG, et al. Prostate cancer: prediction of extracapsular extension with endorectal MR imaging and three-dimensional proton MR spectroscopic imaging. Radiology. 1999;213:481–8. [PubMed: 10551230]
44. Zakian KL, Sircar K, Hricak H, Chen HN, Shukla-Dave A, Eberhardt S, et al. Correlation of proton MR spectroscopic imaging with Gleason score based on step-section pathologic analysis after radical prostatectomy. Radiology. 2005;234(3):804–14. [PubMed: 15734935]
45. Kobus T, Hambrock T, Hulsbergen-van de Kaa CA, Wright AJ, Barentsz JO, Heerschap A, et al. In vivo assessment of prostate cancer aggressiveness using magnetic resonance spectroscopic imaging at 3T with an endorectal coil. Eur Urol. 2011;60:1074–80. [PubMed: 21419565]
46. Shukla-Dave A, Hricak H, Akin O, Yu C, Zakian KL, Udo K, et al. Preoperative nomograms incorporating magnetic resonance imaging and spectroscopy for prediction of insignificant prostate cancer. BJU Int. 2012;109:1315–22. [PubMed: 21933336]
47. Westphalen AC, Reed GD, Vinh PP, Sotto C, Vigneron DB, Kurhanewicz J. Multiparametric 3T endorectal MRI after external beam radiation therapy for prostate cancer. J Magn Reson Imaging. 2012;36:430–7. [PubMed: 22535708]
48. Pucar D, Shukla-Dave A, Hricak H, Moskowitz CS, Kuroiwa K, Olgac S, et al. Prostate cancer: correlation of MR imaging and MR spectroscopy with pathologic findings after radiation therapy – initial experience. Radiology. 2005;236:545–53. [PubMed: 15972335]
49. Zakian KL, Hricak H, Ishill N, Reuter VE, Eberhardt S, Moskowitz CS, et al. An exploratory study of endorectal magnetic resonance imaging and spectroscopy of the prostate as preoperative predictive biomarkers of biochemical relapse after radical prostatectomy. J Urol. 2010;184:2320–7. [PubMed: 20952035]
50. Sciarra A, Panebianco V, Salciccia S, Lisi D, Alfarone A, Gentilucci A, et al. Determination of the time for maximal response to neoadjuvant hormone therapy for prostate cancer using magnetic resonance with spectroscopy (MRSI) and dynamic contrast enhancement (DCEMR). Urol Oncol. 2012;30:614–9. [PubMed: 21396849]
51. Verma S, Turkbey B, Muradyan N, Rajesh A, Cornud F, Haider MA, et al. Overview of dynamic contrast-enhanced MRI in prostate cancer diagnosis and management. AJR Am J Roentgenol. 2012;198:1277–88. [PubMed: 22623539]
52. Haider MA, Chung P, Sweet J, Toi A, Jhaveri K, Ménard C, et al. Dynamic contrast-enhanced magnetic resonance imaging for localization of recurrent prostate cancer after external beam radiotherapy. Int J Radiat Oncol Biol Phys. 2008;70:425–30. [PubMed: 17881141]
53. Puech P, Betrouni N, Makni N, Dewalle AS, Villers A, Lemaitre L. Computer-assisted diagnosis of prostate cancer using DCE-MRI data: design, implementation and preliminary results. Int J Comput Assist Radiol Surg. 2009;4:1–10.
54. Tofts PS, Brix G, Buckley DL, Evelhoch JL, Henderson E, Knopp MV, et al. Estimating kinetic parameters from dynamic contrast-enhanced T1-weighted MRI of a diffusible tracer: standardized quantities and symbols. J Magn Reson Imaging. 1999;10:223–32. [PubMed: 10508281]
55. Ocak I, Bernardo M, Metzger G, Barrett T, Pinto P, Albert PS, et al. Dynamic contrast-enhanced MRI of prostate cancer at 3 T: a study of pharmacokinetic parameters. AJR Am J Roentgenol. 2007;189:849. [PubMed: 17885055]
56. Delongchamps NB, Rouanne M, Flam T, Beuvon F, Liberatore M, Zerbib M, et al. Multiparametric magnetic resonance imaging for the detection and localization of prostate cancer: combination of T2-weighted, dynamic contrast enhanced and diffusion-weighted imaging. BJU Int. 2011;107:1411–8. [PubMed: 21044250]
57. Sella T, Schwartz LH, Swindle PW, Onyebuchi CN, Scardino PT, Scher HI, et al. Suspected local recurrence after radical prostatectomy: endorectal coil MR imaging. Radiology. 2004;231:379–85. [PubMed: 15064390]
58. Shiiba M, Ishihara K, Kimura G, Kuwako T, Yoshihara H, Sato H, et al. Evaluation of primary prostate cancer using 11C-methionine-PET/CT and 18F-FDG-PET/CT. Ann Nucl Med. 2012;26:138–45. [PubMed: 22069194]
59. Minamimoto R, Uemura H, Sano F, Terao H, Nagashima Y, Yamanaka S, et al. The potential of FDG-PET/CT for detecting prostate cancer in patients with an elevated serum PSA level. Ann Nucl Med. 2011;25:21–7. [PubMed: 20931305]

60. Hara T, Kosaka N, Kishi H. PET imaging of prostate cancer using carbon-11-choline. J Nucl Med. 1998;39:990–5. [PubMed: 9627331]
61. Farsad M, Schiavina R, Castellucci P, Nanni C, Corti B, Martorana G, et al. Detection and localization of prostate cancer: correlation of (11)C-choline PET/CT with histopathologic step-section analysis. J Nucl Med. 2005;46:1642–9. [PubMed: 16204714]
62. Eschmann SM, Pfannenberg AC, Rieger A, Aschoff P, Müller M, Paulsen F, et al. Comparison of 11C-choline-PET/CT and whole body-MRI for staging of prostate cancer. Nuklearmedizin. 2007;46:161–8. [PubMed: 17938748]
63. Yamaguchi T, Lee J, Uemura H, Sasaki T, Takahashi N, Oka T, et al. Prostate cancer: a comparative study of 11C-choline PET and MR imaging combined with proton MR spectroscopy. Eur J Nucl Med Mol Imaging. 2005;32:742–8. [PubMed: 16052370]
64. Beer AJ, Eiber M, Souvatzoglou M, Holzapfel K, Ganter C, Weirich G, et al. Restricted water diffusibility as measured by diffusion-weighted MR imaging and choline uptake in (11)C-cho-line PET/CT are correlated in pelvic lymph nodes in patients with prostate cancer. Mol Imaging Biol. 2011;13:352–61. [PubMed: 20490932]
65. Park H, Wood D, Hussain H, Meyer CR, Shah RB, Johnson TD, et al. Introducing parametric fusion PET/MRI of primary prostate cancer. J Nucl Med. 2012;53:546–51. [PubMed: 22419751]
66. Kato T, Tsukamoto E, Kuge Y, Takei T, Shiga T, Shinohara N, et al. Accumulation of [11C]acetate in normal prostate and benign prostatic hyperplasia: comparison with prostate cancer. Eur J Nucl Med Mol Imaging. 2002;29:1492–5. [PubMed: 12397469]
67. Mena E, Turkbey B, Mani H, Adler S, Valera VA, Bernardo M, et al. 11C-Acetate PET/CT in localized prostate cancer: a study with MRI and histopathologic correlation. J Nucl Med. 2012;53:538–45. [PubMed: 22343504]
68. Jambor I, Borra R, Kemppainen J, Lepomäki V, Parkkola R, Dean K, et al. Improved detection of localized prostate cancer using co-registered MRI and 11C-acetate PET/CT. Eur J Radiol. 2012;81:2966–72. [PubMed: 22342610]
69. Jambor I, Borra R, Kemppainen J, Lepomäki V, Parkkola R, Dean K, et al. Functional imaging of localized prostate cancer aggressiveness using 11C-acetate PET/CT and 1H-MR spectroscopy. J Nucl Med. 2010;51:1676–83. [PubMed: 20956477]
70. Wachter S, Tomek S, Kurtaran A, Wachter-Gerstner N, Djavan B, Becherer A, et al. 11C-acetate positron emission tomography imaging and image fusion with computed tomography and magnetic resonance imaging in patients with recurrent prostate cancer. J Clin Oncol. 2006;24:2513–9. [PubMed: 16636343]
71. Schuster DM, Votaw JR, Nieh PT, Yu W, Nye JA, Master V, et al. Initial experience with the radiotracer anti-1-amino-3–18F-fluorocyclobutane-1-carboxylic acid with PET/CT in prostate carcinoma. J Nucl Med. 2007;48:56–63. [PubMed: 17204699]
72. Schuster DM, Savir-Baruch B, Nieh PT, Master VA, Halkar RK, Rossi PJ, et al. Detection of recurrent prostate carcinoma with anti-1-amino-3–18F-fluorocyclobutane-1-carboxylic acid PET/CT and 111In-capromab pendetide SPECT/CT. Radiology. 2011;259:852–61. [PubMed: 21493787]
73. Mosavi F, Johansson S, Sandberg DT, Turesson I, Sörensen J, Ahlström H. Whole-body diffusion-weighted MRI compared with (18)F-NaF PET/CT for detection of bone metastases in patients with high-risk prostate carcinoma. AJR Am J Roentgenol. 2012;199:1114–20. [PubMed: 23096187]
74. Kurdziel KA, Shih JH, Apolo AB, Lindenberg L, Mena E, McKinney YY, et al. The kinetics and reproducibility of 18F-sodium fluoride for oncology using current PET camera technology. J Nucl Med. 2012;53:1175–84. [PubMed: 22728263]

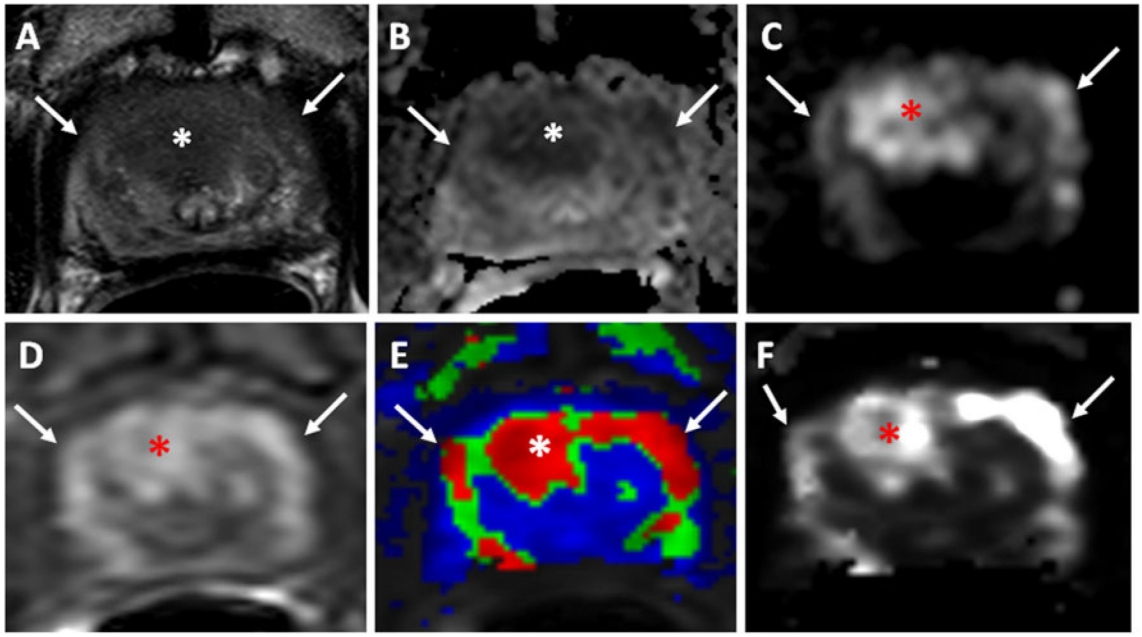

Fig. 1.

A 66-year-old man with a serum PSA of 32 ng/dl. Axial T2-W MR image (**a**), ADC map of DW MRI (**b**), b2,000 DW MR image (**c**), raw DCE MR image (**d**), and k-trans (**e**) and k_{ep} (**f**) maps derived from DCE MRI demonstrate a lesion in the midline anterior central gland (*asterisk*). This lesion also affects the anterior horns of the PZ (*arrows*). Subsequent transrectal ultrasonography/MRI fusion-guided biopsy revealed a Gleason 4+5 (80 %) tumor in the lesion

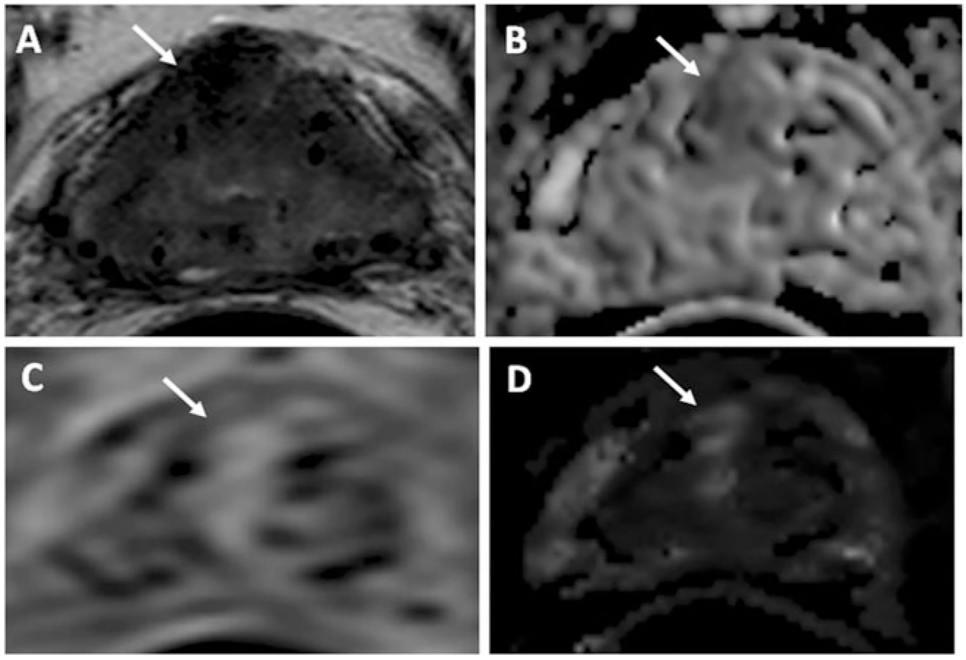

Fig. 2.

A 63-year-old man with a serum PSA of 1.93 ng/dl 6 years after brachytherapy. Axial T2-W MR image (**a**), ADC map of DW MRI (**b**), raw DCE MR image (**c**), and k_{ep} map derived from DCE MRI (**d**) demonstrate a recurrent lesion in the right anterior central gland (*arrow*). Subsequent transrectal ultrasonography/MRI fusion-guided biopsy revealed it to be a Gleason 3+3 (80 %) tumor

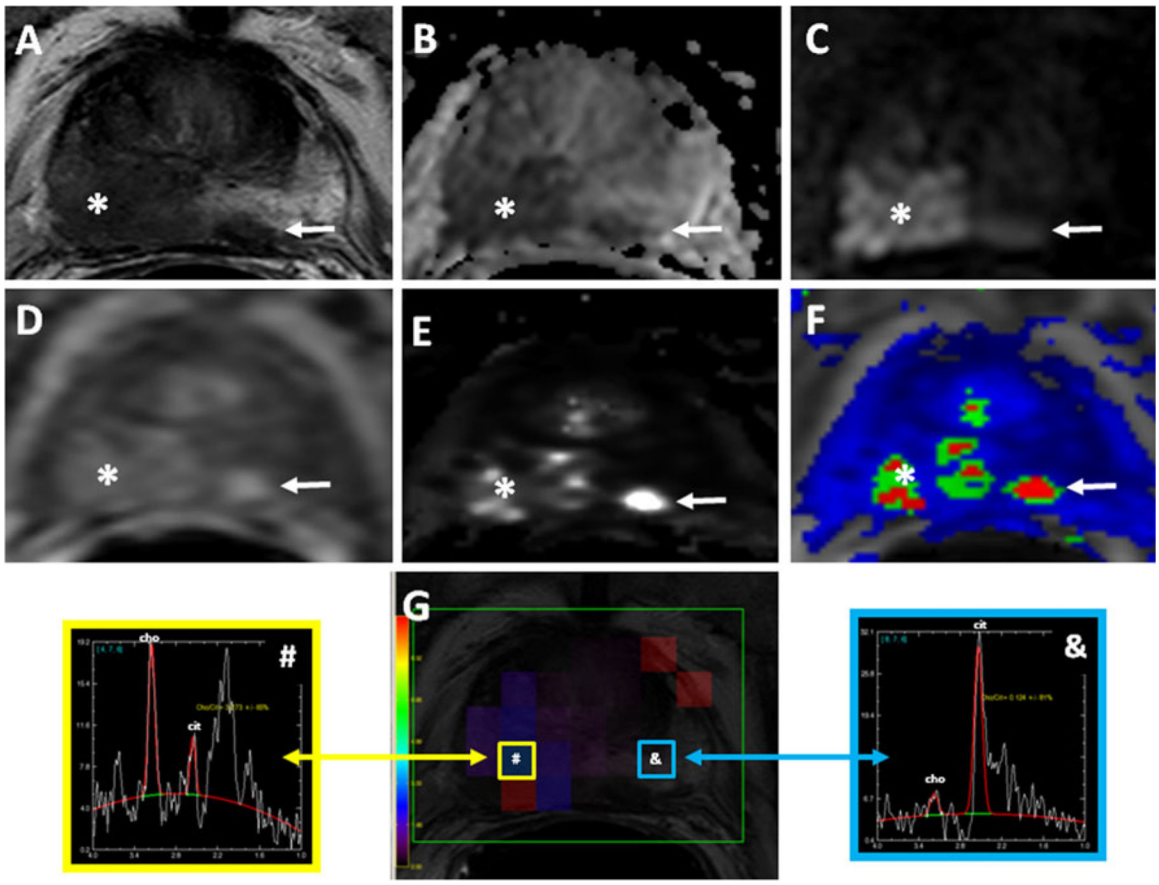

Fig. 3.

A 58-year-old man with a serum PSA of 27 ng/dl with no prior biopsy. Axial T2-W MR image (**a**), ADC map of DW-MRI (**b**), b2,000 DW MR image (**c**), raw DCE MR image (**d**), k_{ep} (**e**) and k-trans (**f**) maps, and MR spectra (**g**) demonstrates a lesion in the right mid-base PZ (*asterisk*). A satellite tumor focus is also present in the left PZ (**a-f** *arrows*). Subsequent transrectal ultrasonography/MRI fusion-guided biopsy revealed a Gleason 4+4 tumor in both lesions

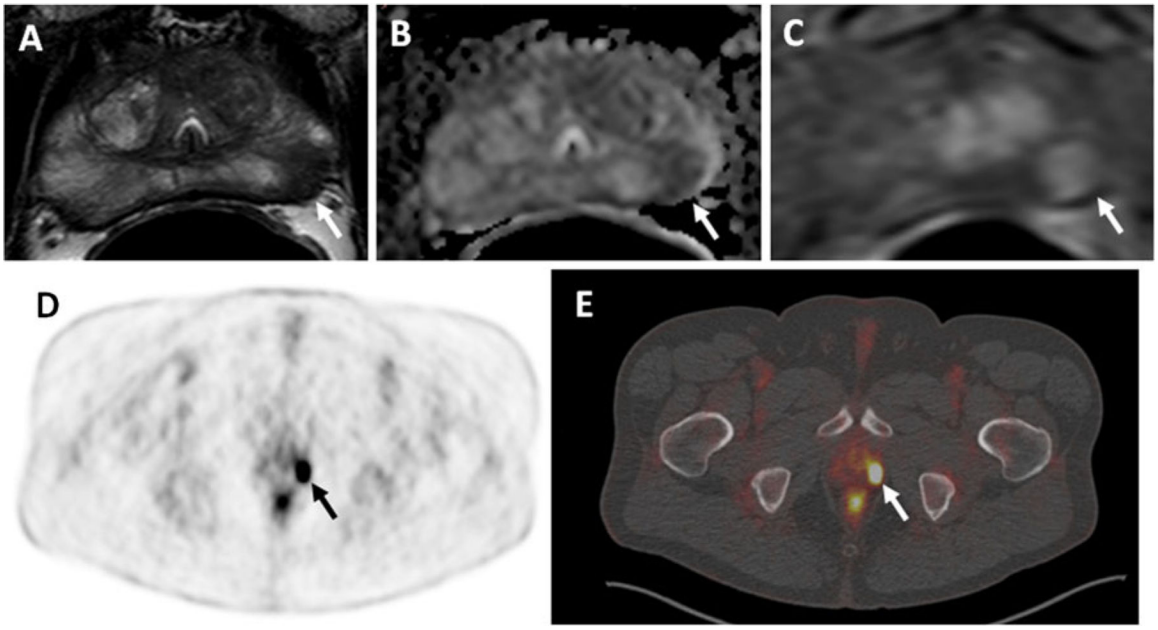

Fig. 4.

A 63-year-old man with a PSA 7 ng/ml. Axial T2-W MR image (**a**), ADC map of DW MRI (**b**) and raw DCE MR image (**c**) demonstrate a lesion in the left apical PZ (*arrows*). Significant uptake of ^{18}F-FDG (*arrows*) is seen in the left-sided lesion in the PET image (**d**) and the hybrid PET/CT image (**e**). Subsequent transrectal ultrasonography/MRI fusion-guided biopsy revealed a Gleason 3+4 tumor in the left apical PZ lesion

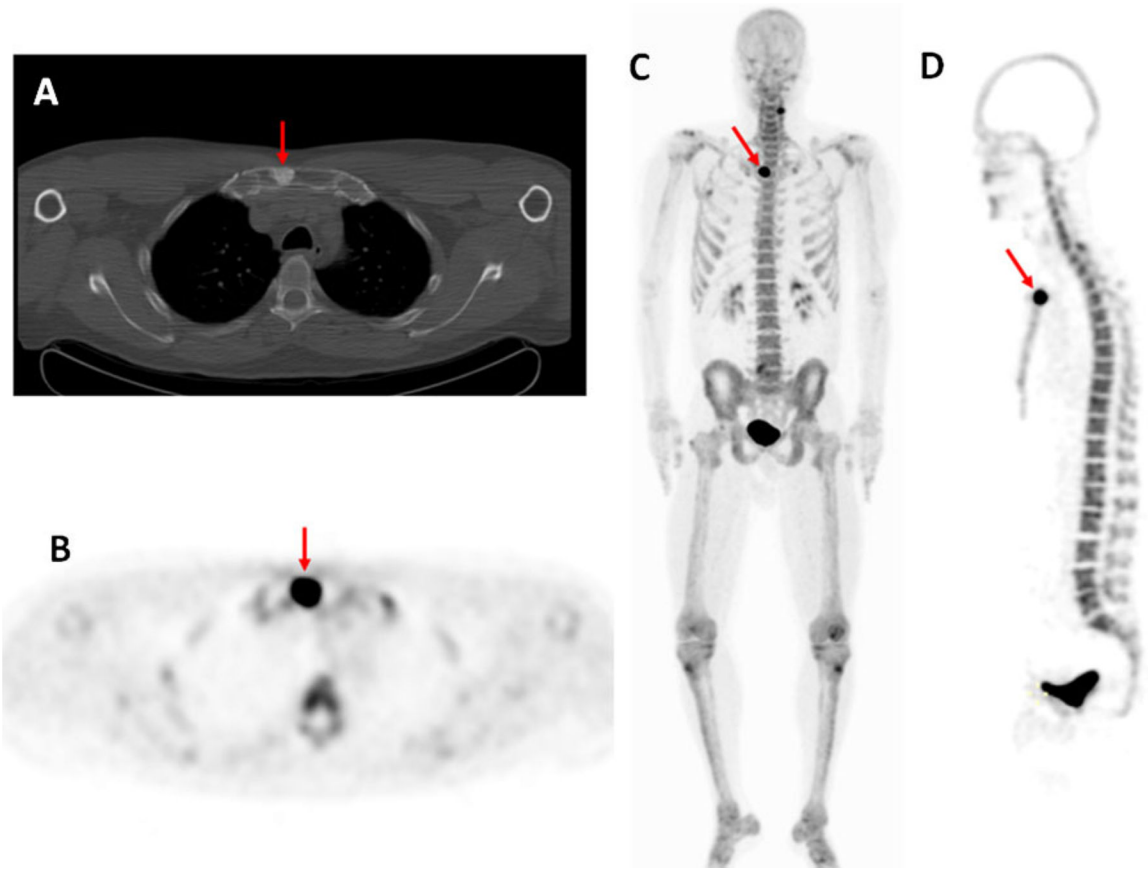

Fig. 5.

A 52 year old man diagnosed with Gleason 4+3 prostate cancer 7 years after radical prostatectomy and salvage radiation with a recent PSA of 2.5 ng/ml. The axial CT image (**a**) demonstrates an osteoblastic lesion in the sternum (*arrow*), and the axial (**b**), coronal (**c**) and sagittal (**d**) maximum intensity projection PET images (obtained at 1 h after injection of ^{18}F-NaF) show increased tracer uptake in the sternal osteoblastic lesion (*arrows*), which is consistent with metastatic disease. Note the uptake in the lateral cervical spine on the left (**c**), which is degenerative based on its location, indicating the relative lack of specificity of ^{18}F-NaF PET imaging